Title: Estimating settlements due to TBM tunnelling

Abstract

Soft-ground Tunnel Boring Machines (TBM) are the preferred solution for construction of long tunnels and linear infrastructure assets, especially in urban areas. TBMs allow the control of tunnel face stability, minimizing effects on the surrounding ground. Unfortunately, existing methods for the assessment of ground surface movements due to TBM tunnelling either utilise complex and computationally expensive numerical analyses or rely on simplistic volume loss theories, which do not consider the characteristics of the ground and TBM operation. This paper presents a simple formulation to estimate the immediate surface settlement due to the applied TBM support pressure, based on an analogy with the hyperbolic behaviour of stress-strain curves of soils. The maximum surface settlement and volume loss were the variables chosen to describe the ground movement while the TBM face support pressure describes the tunnel internal support pressure. Uncertainties due to the inherent variability of geotechnical parameters were also considered, resulting in definition of lower and upper boundaries. Data from a series of centrifuge test results, with and without tunnel face reinforcement by forepoles and a real scale TBM case study were used to validate the proposed model. Presented analyses show that the proposed model adequately represented observed settlement data.

Keywords chosen from ICE Publishing list

Settlement, Tunnels & Tunnelling, Centrifuge Modelling.

1. Introduction

Tunnel Boring Machines (TBMs) for soft ground have become the preferred option for construction of long tunnels in urban areas. Despite the careful operation of TBMs, ground disturbance is inevitable . Leca and New (2007) show that ground movements are induced by tunnelling as a consequence of the development of plastic zone of the groundmass, which is initiated at the tunnel face and propagates into the ground. Even settlements of low magnitude might cause serviceability problems on nearby structures or pipelines (Vorster et al., 2005). Therefore, the estimation of ground movements due to tunnelling is of paramount importance.

Several approaches that do not consider the specific conditions of TBM excavations have been proposed to estimate ground movements, such as empirical methods (Attewell and Woodman, 1982; Celestino et al., 2000; Franza and Marshall, 2019; Jacobsz et al., 2004; New, 1991; Peck, 1969; Vorster et al., 2005), analytical solutions (Litwiszyn, 1957; Sagaseta, 1987; Pinto and Whittle, 2014; Verruijt and Booker, 1996), numerical methods (Avgerinos et al., 2018; Fargnoli et al., 2015; Komiya et al., 1999; Lee and Rowe, 1990; Wongsaroj et al., 2013) or physical modelling (Atkinson and Potts, 1977; Franza et al., 2019; Marshall et al., 2012; Meguid et al., 2008; Schofield, 1980).

Ground movements due to TBM tunnelling are largely associated with plastic behaviour of the groundmass. Therefore, the most common procedures to minimize ground movement are based on methods to stabilize the tunnel face against groundmass instability by applying internal support pressure in the excavation chamber (Mair and Taylor, 1997). The design approach based on controlling ground movements through tunnel face support has led to the development of several methods for the evaluation of excavation stability. These methods, however, do not provide estimations of ground movement. It is simply assumed that a stable excavation would not produce significant settlements. According to Guglielmetti et al. (2008), the main analytical approaches for assessing tunnel face stability are those proposed by: Anagnostou and Kovári (1994, 1996), based on the limit equilibrium method (LEM); Carranza-Torres (2004), based on the Caquot's lower-bound solution of cavity collapse for an elastoplastic Mohr-Coulomb material; and Leca and Dormieux (1990), which is based on the upper-bound solution of plasticity theory. Numerical analysis of TBMs, based mainly on the Finite Element Method, is also employed for evaluating the effect of TBM support pressure in controlling tunnel face stability (Kavvadas et al., 2017).

Despite the large number of methods available for evaluating tunnel face stability, there is a

limited number of methods for the quantitative estimation of ground surface movements due to TBM tunnelling. The short-term analysis of ground response is generally expressed in terms of the maximum surface settlement (S_{max}) and the volume loss (V_L) variables. Ground movement has been empirically related to the stability ratio (N), defined by Broms and Bennermark (1967). Attewell et al. (1986) presented a direct correlation between V_L and N. Macklin (1999) proposed a relationship to estimate V_L based on the concept of Load Factor (L_F) introduced by Mair et al. (1981) using results of centrifuge tests. Later, Atkinson (2007), also based on centrifuge tests, proposed a relation between L_F, V_L, and the applied support pressure.

Osman et al. (2006) proposed a simplified closed-form solution, based on the upper-bound theorem of plasticity, for the prediction of maximum surface ground settlement considering the applied tunnel support pressure. A series of five centrifuge test analyses on plane-strain unlined tunnels in kaolin clay was conducted to validate this formulation. They observed a close correspondence between experimental observations and theoretical predictions for deep tunnels ($C/D > 3$) but poor correlations for shallow tunnels ($C/D < 3$), with C and D defined as in Figure 1.

This brief literature background indicates that there is a need for the development of methods for estimating ground movements due to TBM excavation. In this context, a simplified method based on the general approach presented by Osman et al. (2006) is presented herein. The proposed method relates maximum settlement and volume loss with support pressures using an analogy with the hyperbolic behaviour of stress-strain curves of soils. The proposed approach considers both drained and undrained conditions, but the validation analyses presented herein are limited to centrifuge test under undrained conditions. Furthermore, the definition of lower and upper-bound are proposed to address the inherent variability of soil properties.

2. Proposed model for ground surface settlement

Figure 1 shows a representation of a typical transverse surface settlement curve, S (mm), due to excavation, at a sufficient distance behind the advancing tunnel face. Peck (1969) and later Attewell and Woodman (1982) approximated this behaviour to that of a Gaussian probability density function, as follows:

$$S = S_{\max} \exp\left(-\frac{y^2}{2i^2}\right) \qquad 1.$$

where: S_{max} is the maximum surface settlement (mm); y is the transverse distance (m); i is the point of inflection distance of the settlement trough (m). The value of S_{max} may be estimated by integrating Eq. 1 from minus to positive infinity, resulting in:

$$S_{\max} = \frac{AV_L}{i\sqrt{2\pi}} \quad 2.$$

where: V_L is the volume loss (%) and A is the cross-sectional area of the tunnel (m^2). In general, this approximation has been well accepted for its simplicity.

The groundmass displacement along the longitudinal direction (Figure 2) may be categorized as:

- Face loss (zone “a” in Figure 2): ground movement towards the tunnel face due to stress relief. For TBMs, this is normally associated with a low face pressure;
- Shield loss (zone “b” in Figure 2): ground deformation around the shield due to over-cutting edge combined with a misaligned TBM displacement that may result in radial ground movements and soil shearing;
- Tail void loss and lining loss (zone “c” in Figure 2): the first is due to the gap between the tail of the shield and the final precast lining and the second is associated with the deflection of the lining as the ground pressure increases as a consequence of soil closure on the lining. For tunnels lined with thick pre-cast concrete segments, this is usually considered a minor source of ground displacement; and
- Consolidation (zone “d” in Figure 2): ground displacement due to a new pore-water pressure distribution resulting from changes in the drainage conditions.

When the excavation is made in an uncontrolled manner, larger movements are observed, and their mathematical modelling becomes more difficult due to erratic deformation patterns. However, ground displacements may be minimized when tunnelling is performed in a highly controlled manner. Settlements due to TBM excavation may be controlled by the continuous application of active support pressure given by the TBM face support pressure and grout injection pressure (Guglielmetti et al., 2008; Maidl et al., 2012; Mair, 2008; Mollon et al., 2013).

The first three settlement categories (i.e., zones a, b, and c) result in the “immediate” settlement that occurs as the TBM face moves ahead of the measurement point. This paper deals only with the immediate settlements during TBM tunnelling, in conditions that are predominately considered as undrained but may, in highly permeable materials, occur under drained conditions.

2.1 Immediate surface settlement curve

Based on centrifuge test results, Atkinson (2007) presented a conceptual model of groundmass response due to TBM tunnelling. Figure 3c shows a schematic representation of that model, expressed in terms of the expected behaviour of immediate surface settlement due to the applied TBM support pressure. During tunnelling, if the applied TBM support pressure, P, is equal to the estimated initial support pressure for tunnel face stability, P_0, the surface settlement should be negligible. The initial portion of the settlement curve corresponds to predominantly elastic behaviour. The onset of plastic behaviour is identified as the settlement curve approaches the asymptote given by P_{min}. Relatively larger settlements or even face collapse may occur when the applied TBM support pressure reaches a minimum value, P_{min}, which is not necessarily zero.

In order to represent mathematically the general behaviour shown by Atkinson (2007), a model selection analysis has been performed by Franco (2019). The statistical results indicated that a hyperbolic function, similar to the stress-strain relationship (Figure 3d) proposed by Duncan and Chang (1970), provides best results among the tested models. This formulation is based on the family of hyperbolic equations, as follows:

$$\left(\sigma_1 - \sigma_3\right) = \frac{\varepsilon}{a + b\varepsilon} \qquad 3.$$

where: σ_1 and σ_3 are the major and minor principal stresses, ε is the axial strain, and a and b are best-fit parameters. The hyperbolic equation was used to express the relationship between the tunnel pressure support variables shown in Figure 3c, as follows:

$$\left(\frac{S_{\max}}{D}\right) = \frac{a_S\left(P_0 - P\right)}{b_S\left(P_0 - P\right) - 1} \qquad 4.$$

where: S_{max} is the maximum surface settlement (mm); D is the tunnel diameter (mm); P is the applied TBM support pressure (kPa); P_0 is the estimated initial TBM support pressure for face stability (kPa), corresponding to null displacements, and a_S and b_S are best-fit parameters.

The value of P_0, applied along the tunnel axis, may be estimated based on the limit equilibrium method (Anagnostou and Kovári, 1994, 1996) or based on limit analysis approaches (Carranza-Torres, 2004; Davis et al., 1980), among other methods reviewed by Guglielmetti et al. (2008). Note that, depending on the adopted approach, P_0 is estimated by considering different parameters, such as the

tunnel geometry, the unit weight of the material, the coefficient of lateral earth pressure at rest (k_0); and the shear strength parameters. Regarding the parameter k_0, Franzius et al. (2005) indicated that a higher value of k_0 = 1.5 leads to generate widest settlement trough with too small maximum settlement while a lower value of k_0 = 0.5 generates a narrower settlement trough with increased vertical settlement. This analysis indicated that adopting extreme values of k_0 produce minor impact on the estimation of the surface settlement magnitudes and profile. Note also that the tunnel diameter is considered by means of a normalized variable used in Eq. 4.

The initial slope of the proposed settlement curve is obtained by taking the limit of the curve derivative as P approaches P_0:

$$\frac{\partial}{\partial P}\left(\frac{S_{\max}}{D}\right)\Bigg|_{P\to P_0} = a_S \qquad 5.$$

The asymptotic value of the ultimate stress difference $(P_0 - P)_{ult}$ may be determined by rearranging Equation 4 and taking the following limit of S_{max}:

$$\lim_{S_{\max}\to\infty}\left(\frac{S_{\max}}{b_S S_{\max} - a_S D}\right) = \left(P_0 - P\right)_{ult} = \frac{1}{b_S} \qquad 6.$$

2.2 Relationships between model parameters and geotechnical properties

Based on Equation 5, the following relationships are proposed for the estimation of the parameter a_S, in the drained and undrained conditions in Equations 7 and 8, respectively:

$$a_S = 1/E'_{ur} \qquad 7.$$

$$a_S = 1/E_{ur} \qquad 8.$$

where: E'_{ur} and E_{ur} are the unloading-reloading elastic moduli (kPa) for drained and undrained conditions, respectively.

Figure 3 presents an analogy between a triaxial loading test and the stress path due to TBM tunnelling. Tunnel construction using a TBM often produces a reduced triaxial extension path, which is the reverse form of a conventional triaxial compression. The groundmass may be brought to a state of development of plastic zone by keeping the grout pressure constant, equal to P_0, and decreasing the face pressure to a value equal to P_{min}, as shown in Figure 3e. The asymptotic value $(P_0 - P)_{ult}$ may be related to the stress difference at failure $(P_0 - P_{min})$ using a constant failure ratio R_f inspired in the ratio

proposed by Duncan and Chang (1970):

$$\left(P_0 - P_{\min}\right) = R_f^* \left(P_0 - P\right)_{ult} \quad (9)$$

where: $R^*_f = R_f/(C/D)$. This definition of R^*_f allows the consideration of the influence of the ratio between tunnel cover and diameter (C/D).

Assuming that P_{min} and P_0 are principal stresses and considering a limit state defined by the Mohr-Coulomb envelope, the following expressions for ($P_0 - P_{min}$) are obtained for drained and undrained conditions in Equations 10 and 11, respectively:

$$\left(P_0 - P_{\min}\right) = \frac{2c'\cos\varphi' + 2\left(P_0 - u_{w0}\right)\sin\varphi'}{1+\sin\varphi'} \quad (10)$$

$$\left(P_0 - P_{\min}\right) = 2S_u \quad (11)$$

where: c' is the effective cohesion (kPa); φ' is the effective friction angle (deg.); u_{w0} is the pore-water pressure at the tunnel axis (kPa); and S_u is the undrained shear strength (kPa).

Combining Equations 6, 9, 10, and 11, the following expressions are obtained for the parameter b_S in the drained and undrained conditions, in Equations 12 and 13, respectively:

$$b_S = \frac{1+\sin\varphi'}{2c'\cos\varphi' + 2\left(P_0 - u_{w0}\right)\sin\varphi'} R_f^* \quad (12)$$

$$b_S = \frac{1}{2S_u} R_f^* \quad (13)$$

The proposed simplified approach may also be used in terms of volume loss (V_L). According to Atkinson (2007), V_L is defined as the ratio between the volume of over-excavated material and the tunnel volume per unit distance. Similar to volumetric strain, volume loss is a dimensionless variable. No relation is assumed between these two parameters, since in undrained conditions volumetric strain is null while volume loss is not. The hyperbolic equation may be presented, in terms of volume loss V_L, as follows:

$$V_L = \frac{a_V\left(P_0 - P\right)}{b_V\left(P_0 - P\right) - 1} \quad (14)$$

In a similar manner, the parameters a_V and b_V may be determined based on the elastic modulus and on the limit state, for both drained and undrained conditions, as shown in Eqs. 6, 7, 12, and 13.

The equations in terms of V_L will not be used herein and only the model for S_{max} will be evaluated, exclusively for the undrained condition. It is important to note that the proposed formulation relies on a simplified representation of the complex groundmass stress distribution near the tunnel. Therefore, the procedure proposed herein must be considered semi-empirical.

2.3 Dealing with the variability of input parameters

Some attention has been directed in the past towards the evaluation of how inherent groundmass variability results in scattered ground displacements (Suwansawat and Einstein, 2006; Fargnoli et al., 2013). The variability of geotechnical parameters and ground profile stratigraphy constitute a major source of uncertainty for the assessment of ground movements in TBM tunnelling projects. Thus, an appropriate description of these uncertainties is necessary (Kulhawy, 1992; Phoon and Kulhawy, 1999).

This section presents a simplified approach for the evaluation of the uncertainty of the settlement curve model proposed herein. The indicated procedure is based on the approach proposed by Zhai and Rahardjo (2013), using lower and upper-bound settlement curves. According to Kool et al. (1987), the bounds of a model are directly correlated to the confidence limits of the input parameters. For this study, the parameters a_S and b_S are assumed to be represented by the log-normal probability density function. The lower and upper-bounds are defined by estimating the 10th and 90th percentiles of the probability density function of each variable.

The physical meanings of the parameters a_S and b_S have been clearly defined and their behaviour with respect to S_{max} is exemplified in Figure 4. If each variable is analysed separately, the higher the values of a_S and b_S, the higher the absolute value of S_{max}. Therefore, the lower and upper bounds of the settlement curve should be defined by specific combinations of a_S and b_S, as follows:

$$\left(\frac{S_{\max}}{D}\right)_{upper-bound} = \frac{a_{S90}\left(P_0 - P\right)}{b_{S90}\left(P_0 - P\right) - 1} \quad (15.)$$

$$\left(\frac{S_{\max}}{D}\right)_{lower-bound} = \frac{a_{S10}\left(P_0 - P\right)}{b_{S10}\left(P_0 - P\right) - 1} \quad (16.)$$

where a_{S90} and b_{S90} correspond to the 90th percentile and a_{S10} and b_{S10} correspond to the 10th percentile.

From a practical point of view in the tunnelling industry, the above approach might be considered as complementary tool to be used in the protocol of tunnel excavation for defining the attention and

alarm limits of support pressure likely to occur during tunnelling as well as the immediate settlements that the support pressure might induced.

3. Analysis of centrifuge tests

The following section presents the analysis of previously published results of centrifuge tests carried out in undrained conditions, with and without the reinforcement of the tunnel face by forepoles. The hyperbolic model (Eq. 4) is used to evaluate surface settlements as a function of support pressure. Table 1 summarizes the features of each reference centrifuge test result collected from the literature. Basic input information regarding the geometry of each centrifuge model and the geotechnical properties are indicated. Unfortunately, only one reference presents information regarding the unloading-reloading total elastic modulus, E_{ur}.

Figures 5 and 6 show experimental and modelling results of the centrifuge tests carried out by Lee and Rowe (1989) and Osman et al. (2006), all without tunnel face reinforcement. A value of P_0 of 130 kPa was considered for each test. The tests involved different values of overburden depth (C) and tunnel diameter ratio (C/D). Table 2 presents the best-fit values of a_S and b_S, obtained from nonlinear regression analyses. The values of number of data points (n) and standard error (SE) for each variable are also presented for each test. The values of coefficient of determination (R^2) and of Root Mean Square Error (RMSE) indicate excellent agreement between the experimental data and the model, with R^2 values ranging between 0.942 and 0.995.

Figure 7 shows a series of eight two-dimensional plane strain centrifuge model tests performed by Divall et al. (2016). These tests were designed to investigate how forepoles affect the plastic collapse mechanism surrounding a tunnel excavation in stiff clay. These results allow the evaluation, using the proposed model, of how different forepole arrangements may artificially improve the soil around tunnel and might affect the surface settlement behaviour. However, a detailed analysis of the behaviour of the forepoles themselves is beyond the scope of this paper.

Divall et al. (2016) simulated the excavation by reducing the pressure, starting from an average initial support pressure of 211 kPa. However, the test results indicated negligible ground response up to a support pressure of 160 kPa, probably because P_0 was estimated as a function of the original soil condition (i.e., without the influence of forepoles). To address this inconsistency, the formulation proposed by Broms and Bennermark (1967) was employed:

$$N = \frac{\gamma\left(C + D/2\right) + \sigma_S - \sigma_T}{S_u} \quad (17)$$

where: γ = 17.5 kN/m³ (Divall, 2013); σ_S = 0 is the surface surcharge pressure; S_u = 30 kPa; and σ_T = P_0.

Sensitivity analyses showed that values of N = 2 and P_0 = 160 kPa represented adequately the centrifuge data. Therefore, a value of P_0 = 160 kPa was assumed in the modelling exercises presented herein. Figure 7 shows, for all centrifuge arrangements, that the proposed model agrees with the test results. The obtained coefficients of determination were higher than 0.99 for five out of eight tests.

Table 2 presents a comparison between the geotechnical parameters reported by the original references and the respective values estimated using Eqs. 8 and 13 and the best-fit parameters for Eq. 4. The adopted value of R_f was 0.9 for all the tests with clays. Lee and Rowe (1989) are the only reference that presents the value of E_{ur}, which is in close agreement with the model prediction. Regarding S_u, most measured values were adequately predicted, with a maximum relative error of 15%. The lower agreement observed for tests FP4, FP5 and FP7 from Divall et al. (2016) may be explained by the higher values of surface settlement as collapse approaches, with a support pressure below 20 kPa. This is an obvious indication that the arrangements of forepoles may contribute to reinforce the soil around the excavation. A Pearson correlation analysis of measured and predicted values of E_{ur} and S_u, especially from the tests results performed by Divall et al. (2016), showed a correlation of r = 0.6149, which indicates a moderate tendency for correlation. The lack of a strong correlation might be attributed to the fact that the soil was artificially improved by the addition of forepoles.

The new formulation provided an accurate fitting of the ground surface movement with the applied TBM support pressure as well as a consistent estimation of geotechnical parameters. Even though the analyses with the tunnel face reinforced by forepoles are mainly used in practice with open face tunnelling and not for TBMs, the formulation also demonstrates, in terms of the predicted values of equivalent S_u, the effectiveness of the forepoles as soil reinforcement around a tunnel heading.

4. Case study – Line 5 of São Paulo Metro

The proposed procedure for incorporating the uncertainty of input parameters in the evaluation of settlement curves has been applied to a case study. The tunnel project corresponds to a 11.5 km long new extension of Line 5 of Sao Paulo Metro, located in the densely populated south region of the city

of Sao Paulo, Brazil (Figure 8). The new extension involves the construction of eleven stations and thirteen ventilation shafts, among other structures and facilities. The line extension was excavated by three Earth Pressure Balance (EPB) machines, two small EPB machines of 6.90 m in diameter, for two single track tunnels between Adolfo Pinheiro and Eucalipto stations, and one large EPB machine of 10.60 m in diameter, for a double track tunnel between Eucalipto and Chacara Klabin stations. The case study presented herein concerns the tunnel excavation by the larger EPB machine, specifically, in a 670 m stretch of the tunnel line, located between Hospital Sao Paulo (HSP) and Santa Cruz (SCR) stations. The tunnel cover depth in this section is of 24.35 m.

In terms of site geology, the line in this section crosses the Resende Formation, which comprises basal and sedimentary units of the Taubaté Group from the Eocene Period. It consists of a system of alluvial beds associated with the fluvial plain of intertwined rivers. This formation comprises two main lithofacies. The first lithofacy corresponds to the proximal alluvial beds, located in the vicinity of the contact with the basement, composed of polymitic conglomerates, interdigitated with sandstones and sandy mudstones. The second lithofacy corresponds to the alluvial beds in distal position associated to intertwined rivers, with occurrence of sandstones intercalated with mudstones. Detrital smectites (argillomineral of the expansive type) are present, which are considered as indicators of climatic semi-aridity and ineffective drainage.

The cover to diameter ratio (C=D) is constant along the tunnel stretch, with a value of 2.30. Further details about this case study are presented by Franco et al. (2019).

Table 3 shows the observed maximum surface settlements (S_{max}) and applied TBM support pressures (P) for each of the nineteen monitoring cross-sections. A relatively high variability is observed for S_{max}, which was expressed in terms of the coefficient of variation (CoV). Franco (2019) performed an analysis for the estimation of P_0 by following the limit equilibrium procedures proposed by Anagnostou and Kovári (1994) and considering drained conditions. The groundmass has four different soil types forming six layers, each layer with variable thickness. The values of C and D are 24.35 m and 10.60 m, respectively. The estimated value of P_0, in terms of total stress, was 308 kPa. Figure 9 and Table 4 show the tunnel model geometry, and the mean soil property values, respectively, considered in the case study for the estimation of P_0.

Figure 10 shows the best-fit results using the proposed model. The best-fit values for parameters $D.a_S$ and b_S, obtained based on the monitored data, were equal to 0.02550 mm/kPa and 0.00285 1/kPa,

304 respectively. Figure 10 also shows the lower and upper-bound curves of the proposed model,
305 expressed in terms of the 10th and 90th percentiles, as proposed in Equation 18. Values of CoV between
306 10% and 46% were used to illustrate the variability of the model according to the variability of S_{max}
307 presented in Table 3. A value of CoV of 46% provides an adequate estimation of the lower and upper
308 bounds of the observed values. Therefore, the proposed model may be an acceptable indicator for
309 defining the limits in which soil variability affects the development of ground surface response during
310 TBM tunnelling.
311
312 **5. Concluding remarks**
313 In this paper a simple and practical model for the estimation of ground surface settlements due to TBM
314 tunnelling has been proposed, for both drained and undrained conditions. A series of centrifuge test
315 analyses was used to validate the proposed model. Furthermore, the case study of the new extension
316 of Line 5 of Sao Paulo metro was used to exemplify the determination of the settlement curve in
317 statistical terms, using lower and upper bounds.
318 The physical meaning of the model parameters, a_S and b_S, was demonstrated. In addition, an
319 alternative procedure for the estimation of these parameters was proposed, based on the soil stiffness,
320 shear strength, and initial tunnel support pressure. This semi-empirical estimation procedure is based
321 on an analogy between the stress states in the tunnel cavity and in triaxial tests. The parameter
322 estimation procedure depends on the tunnel cross- section that is under analysis. Therefore, to consider
323 P_0 along a tunnel stretch, the soil stratification must be constant, and the mean values of geotechnical
324 parameter should be considered along the tunnel path, for the ease of calculation.
325 The proposed approach was verified for geometrical conditions in which $C/D < 3$. Centrifuge tests
326 performed by Lee and Rowe (1989) and later by Osman et al. (2006) for $C/D > 3$ show that the
327 settlement curve presents a second inflection point, which may not be adequately represented by the
328 hyperbolic curves. Therefore, the formulation proposed herein should be applied with greater care for
329 deeper tunnels, with C/D > 3.
330 The proposed model offers a valuable tool for TBM tunnelling projects incorporating the support
331 pressure in the calculation of the tunnelling impact. In addition, the input parameters are based on
332 relatively simple standard tests. Finally, it is important to note that the proposed approach can be used
333 to derive lower and upper limits in order to consider the complexity and large number of variables that

affect groundmass response.

Acknowledgements

The authors are grateful to the Companhia do Metropolitano de Sao Paulo (METRO) for providing and authorizing the use of the data in this study, especially Eng. Hugo Rocha. This study was financed in part by the Conselho Nacional de Desenvolvimento Científico e Tecnológico – CNPq.

References

Anagnostou G and Kovári K (1994) The face stability of slurry-shield-driven tunnels. Tunnelling and Underground Space Technology 9(2): 165 – 174.

Anagnostou G and Kovári K (1996) Face stability conditions with earth-pressure-balanced shields. Tunnelling and Underground Space Technology 11(2): 165 – 173.

Atkinson J (2007) The mechanics of soils and foundations. CRC Press.

Atkinson JH and Potts DM (1977) Subsidence above shallow tunnels in soft ground. Journal of Geotechnical and Geoenvironmental Engineering 103 (Proc. Paper 11318 Proceeding).

Attewell B and Woodman P (1982) Predicting the dynamics of ground settlement and its derivatives caused by tunneling in soil 15(8): 13–22.

Avgerinos V, Potts DM, Standing JR and Wan MSP (2018) Predicting tunnelling-induced ground movements and interpreting field measurements using numerical analysis: Crossrail case study at hyde park. Géotechnique 68(1): 31–49.

Broms BB and Bennermark H (1967) Stability of clay at vertical openings. Journal of Soil Mechanics & Foundations Div.

Carranza-Torres C (2004) Computation of Factor of Safety for Shallow Tunnels using Caquot's Lower Bound Solution. Technical report, Technical Report for Geodata.

Celestino T, Gomes R and Bortolucci A (2000) Errors in ground distortions due to settlement trough adjustment. Tunnelling and Underground Space Technology 15(1): 97 – 100.

Davis EH, Gunn MJ, Mair RJ and Seneviratine HN (1980) The stability of shallow tunnels and underground openings in cohesive material. Géotechnique 30(4): 397–416.

Divall S (2013) Ground movements associated with twin-tunnel construction in clay. PhD thesis, City University London.

364 Divall S, Taylor RN and Xu M (2016) Centrifuge modelling of tunnelling with forepoling. International
365 Journal of Physical Modelling in Geotechnics 16(2): 83–95.
366 Duncan JM and Chang CY (1970) Nonlinear analysis of stress and strain in soils. Journal of Soil
367 Mechanics & Foundations Div.
368 Fargnoli V, Boldini D and Amorosi A (2013) Tbm tunnelling-induced settlements in coarse-grained soils:
369 The case of the new milan underground line 5. Tunnelling and Underground Space Technology 38:
370 336 – 347.
371 Fargnoli V, Gragnano C, Boldini D and Amorosi A (2015) 3d numerical modelling of soil–structure
372 interaction during epb tunnelling. Géotechnique 65(1): 23–37.
373 Franco V (2019) Mathematical and probabilistic modeling approach for estimation of surface
374 settlements due to TBM tunneling. PhD thesis, Department of Civil and Environmental Engineering,
375 Universidade de Bras´ılia, DF, Brasília, 159p.
376 Franco VH, de F.N. Gitirana Jr. and de Assis AP (2019) Probabilistic assessment of tunneling-induced
377 building damage. Computers and Geotechnics 113: 103097.
378 Franza A and Marshall AM (2019) Empirical and semi-analytical methods for evaluating tunnelling-
379 induced ground movements in sands. Tunnelling and Underground Space Technology 88: 47 – 62.
380 Franza A, Marshall AM and Zhou B (2019) Greenfield tunnelling in sands: the effects of soil density and
381 relative depth. Géotechnique 69(4): 297–307.
382 Franzius JN, Potts DM and Burland JB (2005). The influence of soil anisotropy and K_0 on ground surface
383 movements resulting from tunnel excavation. Géotechnique, 55 (3): 189–199.
384 Guglielmetti V, Grasso P, Mahtab A and Xu S (2008) Mechanized Tunnelling in Urban Areas: Design
385 methodology and construction control. Taylor & Francis.
386 Jacobsz SW, Standing JR, Mair RJ, Hagiwara T and Sugiyama T (2004) Centrifuge modelling of
387 tunnelling near driven piles. SOILS AND FOUNDATIONS 44(1): 49–56.
388 Kavvadas M, Litsas D, Vazaios I and Fortsakis P (2017) Development of a 3d finite element model for
389 shield epb tunnelling. Tunnelling and Underground Space Technology 65: 22 – 34.
390 Komiya K, Soga K, Akagi H, Hagiwara T and Bolton MD (1999) Finite element modelling of excavation
391 and advancement processes of a shield tunnelling machine. SOILS AND FOUNDATIONS 39(3):
392 37–52.
393 Kool J, Parker J and van Genuchten M (1987) Parameter estimation for unsaturated flow and transport

394 models — a review. Journal of Hydrology 91(3): 255 – 293.
395 Kulhawy FH (1992) On the evaluation of static soil properties. In Stability and performance of slopes
396 and embankments II, ASCE, pp. 95–115.
397 Leca E and Dormieux L (1990) Upper and lower bound solutions for the face stability of shallow circular
398 tunnels in frictional material. G´eotechnique 40(4): 581–606.
399 Leca E and New B (2007) Settlements induced by tunneling in soft ground. Tunnelling and Underground
400 Space Technology 22(2): 119 – 149.
401 Lee K and Rowe R (1990) Finite element modelling of the three-dimensional ground deformations due
402 to tunnelling in soft cohesive soils: Part i— method of analysis. Computers and Geotechnics 10(2):
403 87 – 109.
404 Lee KM and Rowe RK (1989) Deformations caused by surface loading and tunnelling: the role of elastic
405 anisotropy. Géotechnique 39(1): 125–140.
406 Litwiszyn J (1957) The theories and model research of movements of ground masses. In Proceedings
407 of European Congress Ground Movement, Leeds, Uk, pp. 203–209.
408 Macklin S (1999) The prediction of volume loss due to tunnelling in overconsolidated clay based on
409 heading geometry and stability number. Ground engineering 32(4): 30–33.
410 Maidl B, Herrenknecht M, Maidl U, Wehrmeyer G and Sturge D (2012) Mechanised Shield Tunnelling.
411 John Wiley & Sons.
412 Mair R and Taylor R (1997) Theme lecture: Bored tunnelling in the urban environment. In Proceedings
413 of the fourteenth international conference on soil mechanics and foundation engineering (Hamburg,
414 1997), Balkema, pp. 2353–2385.
415 Mair RJ (2008) Tunnelling and geotechnics: new horizons. Géotechnique 58(9): 695–736.
416 Mair RJ, Gunn MJ and O'Reilly MP (1981) Ground movements around shallow tunnels in soft clay. In
417 Proc. 10th Int. Conf. Soil Mech. and Found. Eng, vol. 1, pp. 323–328.
418 Marshall AM, Farrell R, Klar A and Mair R (2012) Tunnels in sands: the effect of size, depth and volume
419 loss on greenfield displacements. Géotechnique 62(5): 385–399.
420 Meguid M, Saada O, Nunes M and Mattar J (2008) Physical modeling of tunnels in soft ground: A
421 review. Tunnelling and Underground Space Technology 23(2): 185 – 198.
422 Mollon G, Dias D and Soubra AH (2013) Probabilistic analyses of tunneling-induced ground
423 movements. Acta Geotechnica 8(2): 181–199.

New BM (1991) Tunnelling induced ground movements: predicting their magnitude and effects. In 4th Int. Conf. Ground Movements and Structures, Pentech Press, pp. 671–697.

Osman AS, Bolton MD and Mair RJ (2006) Predicting 2d ground movements around tunnels in undrained clay. Géotechnique 56(9): 597–604.

Peck RB (1969) Deep excavations and tunneling in soft ground. In: Proc. 7th International Conference on Soil Mechanics and Foundation Engineering, Mexico City, State of the Art Volume: 225–290.

Phoon KK and Kulhawy FH (1999) Characterization of geotechnical variability. Canadian Geotechnical Journal 36(4): 612–624.

Pinto F and Whittle AJ (2014) Ground movements due to shallow tunnels in soft ground. i: Analytical solutions. Journal of Geotechnical and Geoenvironmental Engineering 140(4): 04013040.

Sagaseta C (1987) Analysis of undraind soil deformation due to ground loss. Géotechnique 37(3): 301–320.

Schofield AN (1980) Cambridge geotechnical centrifuge operations. Géotechnique 30(3): 227–268.

Suwansawat S and Einstein HH (2006) Artificial neural networks for predicting the maximum surface settlement caused by epb shield tunneling. Tunnelling and Underground Space Technology 21(2): 133 – 150.

Verruijt A and Booker JR (1996) Surface settlements due to deformation of a tunnel in an elastic half plane. Géotechnique 46(4): 753–756.

Vorster TE, Klar A, Soga K and Mair RJ (2005) Estimating the effects of tunneling on existing pipelines. Journal of Geotechnical and Geoenvironmental Engineering 131(11): 1399–1410.

Wongsaroj J, Soga K and Mair R (2013) Tunnelling-induced consolidation settlements in london clay. Géotechnique 63(13): 1103–1115.

Zhai Q and Rahardjo H (2013) Quantification of uncertainties in soil–water characteristic curve associated with fitting parameters. Engineering Geology 163: 144 – 152.

Notation list

A	: is the cross-sectional area of the tunnel.
a_S, b_S	: are best-fit parameters for the surface settlement curve.
a_{S90}, b_{S90}	: are best-fit parameters of 90th percentile for the surface settlement curve.
a_{S10}, b_{S10}	: are best-fit parameters of 10th percentile for the surface settlement curve.
a_V, b_V	: are best-fit parameters for the volume loss curve.
C	: is the tunnel cover depth.
CoV	: is the coefficient of variation.
c'	: is the effective cohesion.
D	: is the tunnel diameter.
E'_{ur}	: is the unloading-reloading elastic modulus for drained condition.
E_{ur}	: is the unloading-reloading elastic modulus for undrained condition.
I	: is the point of inflection distance of the settlement trough.
k_0	: is the coefficient of lateral earth pressure at rest.
L_F	: is the load factor.
N	: is the stability ratio.
P	: is the applied TBM support pressure.
P_0	: is the estimated initial TBM support pressure for face stability.
P_{min}	: is the minimum applied TBM support pressure before face collapse may occur.
$(P_0 - P)_{ult}$	: is the ultimate stress difference.
R_f	: is the constant failure ratio proposed by Duncan and Chang (1970).
R^*_f	: is a modification of constant failure ratio.
S	: is the transverse settlement trough curve.
S_{max}	: is the maximum surface settlement.
S_u	: is the undrained shear strength.
V_L	: is the volume loss.
γ	: is the specific weight.
ε	: is the axial strain.
σ_1	: is the major principal stress.
σ_3	: is the minor principal stress.

484 σ_S : is the surcharged load.

485 σ_T : is the tunnel pressure.

486 φ' : is the effective friction angle.

487

488

489

490

491

492

493

494

495

496

497

498

499

500

501

502

503

504

505

506

507

508

509

510

511

512

513

Table captions

Table 1. Data selected from the literature on centrifuge geotechnical tests and reported geotechnical parameters under undrained condition.

Table 2. Best-fit and geotechnical parameters under undrained condition, estimated based on the proposed approach.

Table 3. Mean and CoV values of maximum surface settlement and applied TBM support pressure between HSP and SCR stations.

Table 4. Input geotechnical parameters between HSP and SCR stations (after Franco et al., 2019).

Figure captions

Figure 1. Typical representation of transverse surface settlement.

Figure 2. Sources of longitudinal ground movements due to TBM tunnelling.

Figure 3. Comparison of stress paths: a) tunnel excavation producing reduced triaxial extension; b) conventional triaxial compression; c) settlement curve caused by tunneling; d) triaxial loading curve; and e) shear strength envelope.

Figure 4. Relationships between maximum surface settlement, S_{max}, and the fitting parameters: a) a_S; and b) b_S.

Figure 5. Surface settlement data from Lee and Rowe (1989) and corresponding best-fit modelling.

Figure 6. Surface settlement data from Osman et al. (2006) and corresponding best-fit modelling.

Figure 7. Surface settlement data for the different forepoling arrangements in centrifuge tests from Divall et al. (2016) and corresponding best-fit modelling: a) FP4 and FP8; b) FP2 and FP6; c) FP5 and FP7; d) FP3 and FP9.

Figure 8. Metro stations layout of Line 5.

Figure 9. Tunnel model geometry (modified from Franco et al., 2019).

Figure 10. Upper and lower bounds of S_{max} between stations HSP and SCR.

Tables

Table 1. Data selected from the literature on centrifuge geotechnical tests and reported geotechnical parameters under undrained condition.

Reference	Test ID	(C/D)	D (mm) [m]*	Scale Factor N	Geotechnical parameters	
					E_{ur} (kPa)	S_u (kPa)
Lee and Rowe (1989)	2DP	1.67	36 [4.5]	125	3640	25.3
Osman *et al.,* (2006)	2DH	1.80	60 [4.5]	75	-	26.0
	2DP	1.67	60 [4.5]	75	-	22.6
	2DT	1.67	36[4.5]	125	-	22.6
Divall *et al.,* (2016)	FP2	2.00	50 [5.0]	100	-	33.7
	FP3				-	30.7
	FP4				-	35.0
	FP5				-	34.3
	FP6				-	32.8
	FP7				-	33.1
	FP8				-	32.1
	FP9				-	35.3

* The values in brackets correspond to the full-scale diameter, in meters.

Table 2. Best-fit and geotechnical parameters under undrained condition, estimated based on the proposed approach.

Reference	Test ID	R_f^*	Best-fit parameters		n	Standard Error (SE)		R^2	RMSE	Geotechnical parameters	
			$a_S D$	b_S		P (kPa)	S_{max} (mm)			E_{ur} (kPa)	S_u (kPa)
Lee and Rowe (1989)	2DP	0.54	0.01040	0.01180	21	4.5934	0.3751	0.993	0.142	3462	22.8
Osman *et al.* (2006)	2DH	0.50	0.01690	0.01050	8	7.9040	0.5666	0.988	0.151	3550	23.8
	2DP	0.54	0.01740	0.01190	20	4.7783	0.6407	0.995	0.198	3448	22.6
	2DT	0.54	0.00890	0.01355	18	4.4887	0.3796	0.988	0.171	4045	19.9
Divall *et al.* (2016)	FP2	0.45	0.00422	0.00665	115	3.4845	0.0877	0.996	0.056	11848	33.8
	FP3		0.00525	0.00699	94	3.6095	0.1039	0.994	0.079	4762	32.2
	FP4		0.00395	0.00715	65	4.6069	0.1523	0.833	0.497	12658	31.5
	FP5		0.00199	0.00568	141	4.8731	0.1676	0.915	0.577	25126	39.6
	FP6		0.00525	0.00722	74	4.2731	0.1440	0.993	0.102	9524	31.2
	FP7		0.00118	0.00596	155	3.6571	0.0320	0.966	0.074	42373	37.1
	FP8		0.00655	0.00687	112	3.3305	0.0942	0.994	0.076	7634	32.8
	FP9		0.00545	0.00602	70	4.8642	0.1302	0.995	0.074	9174	37.4

562

563 Table 3. Mean and CoV values of maximum surface settlement and applied TBM support pressure between HSP and SCR stations.

Section number	Monitoring sections	S_{max} (mm)	P (kPa)
1	SC_19+138	1.6	224.00
2	SC_19+162	1.6	237.00
3	SC_19+187	2.3	239.00
4	SC_19+210	1.9	265.00
5	SC_19+234	0.6	260.00
6	SC_19+260	0.7	246.00
7	SC_19+336	3.5	211.00
8	SC_19+400	4.7	199.00
9	SC_19+415	3.5	199.00
10	SC_19+438	3.0	203.00
11	SC_19+461	2.6	207.00
12	SC_19+486	2.7	215.00
13	SC_19+512	3.5	227.00
14	SC_19+560	1.4	238.00
15	SC_19+581	1.6	235.00
16	SC_19+634	3.4	249.00
17	SC_19+658	4.0	239.00
18	SC_19+682	4.8	240.00
19	SC_19+708	3.7	232.00
μ		2.7	229.74
σ		1.3	19.66
CoV	(%)	48.15	8.56

564

565

566

567 Table 4. Input geotechnical parameters between HSP and SCR stations (after Franco et al., 2019).

Geotechnical parameters		**$3A_{gp1}$**	**$3A_{g1.2}$**	**$3A_{r1.2}$**	**$4A_{g1}$**
γ	kN/m^3	16.6	18.5	19.5	20.2
c'	kPa	18	40	7	80
j'	deg	24	24	32	26
E	MPa	20	120	185	230
n	-	0.26	0.30	0.31	0.28
k_0	-	0.67	0.93	0.82	0.90

568

569

Figures

Figure 1. Typical representation of transverse surface settlement.

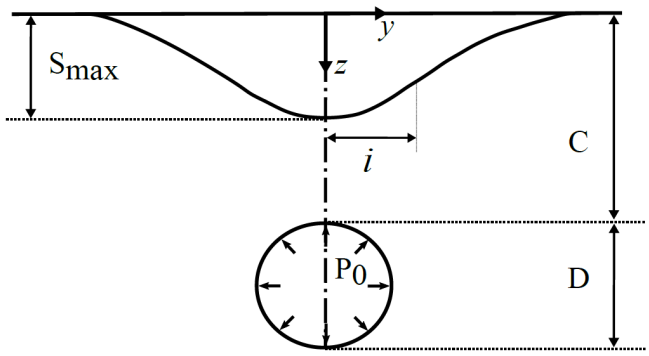

Figure 2. Sources of longitudinal ground movements due to TBM tunnelling.

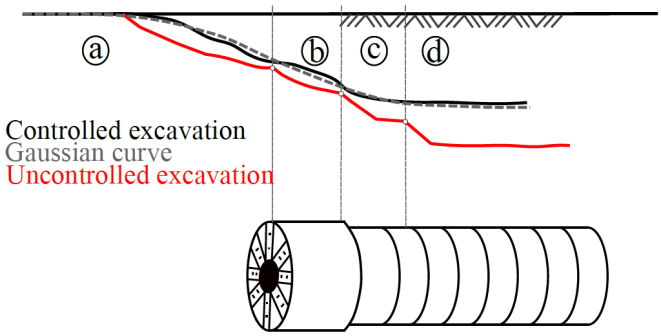

Figure 3. Comparison of stress paths: a) tunnel excavation producing reduced triaxial extension; b) conventional triaxial compression; c) settlement curve caused by tunneling; d) triaxial loading curve; and e) shear strength envelope.

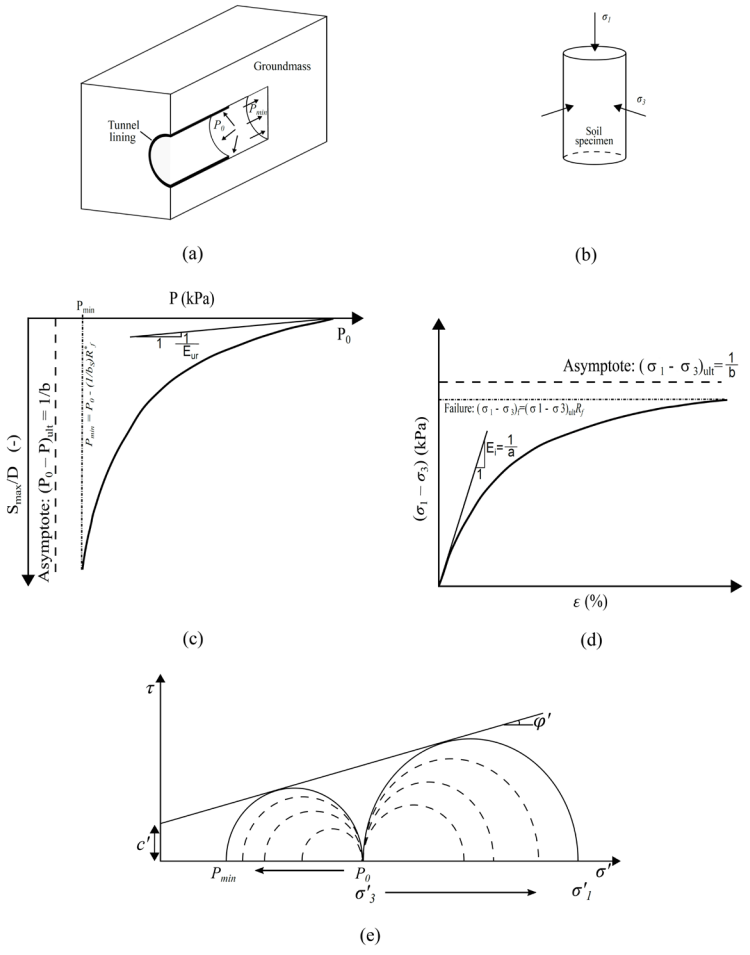

Figure 4. Relationships between maximum surface settlement, S_{max}, and the fitting parameters: a) a_S; and b) b_S.

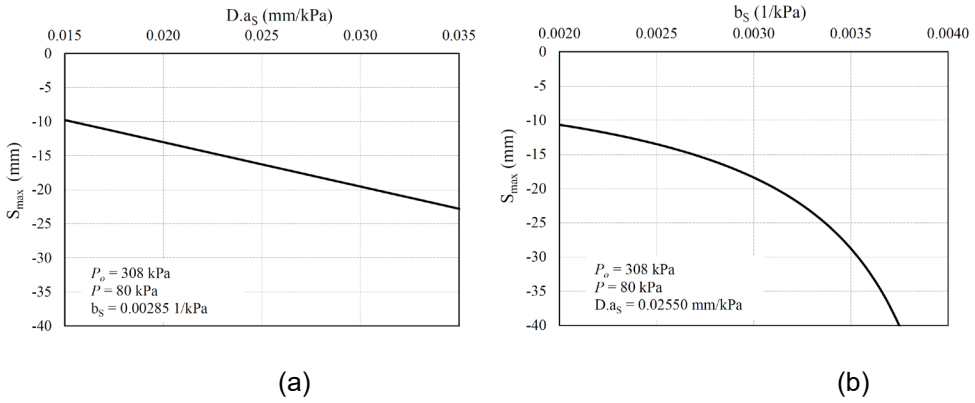

Figure 5. Surface settlement data from Lee and Rowe (1989) and corresponding best-fit modelling.

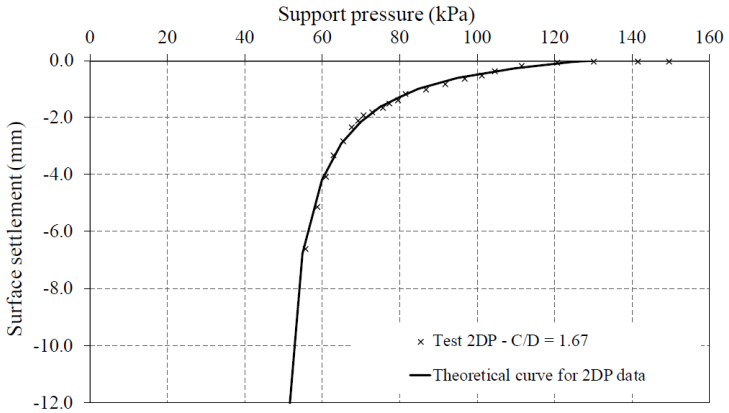

Figure 6. Surface settlement data from Osman et al. (2006) and corresponding best-fit modelling.

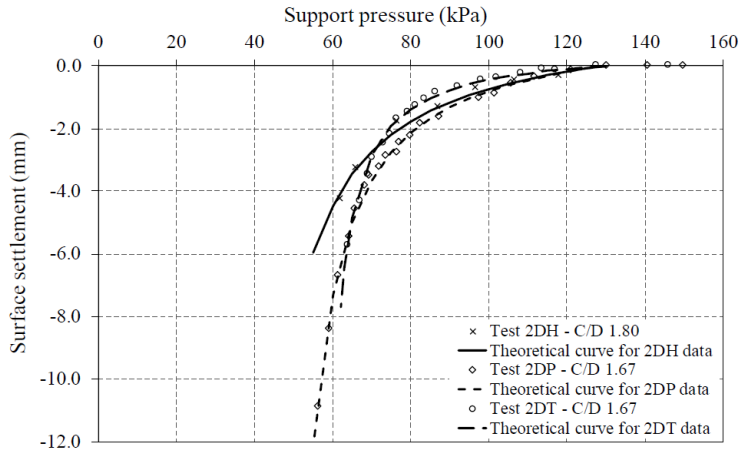

Figure 7. Surface settlement data for the different forepoling arrangements in centrifuge tests from Divall et al. (2016) and corresponding best-fit modelling: a) FP4 and FP8; b) FP2 and FP6; c) FP5 and FP7; d) FP3 and FP9.

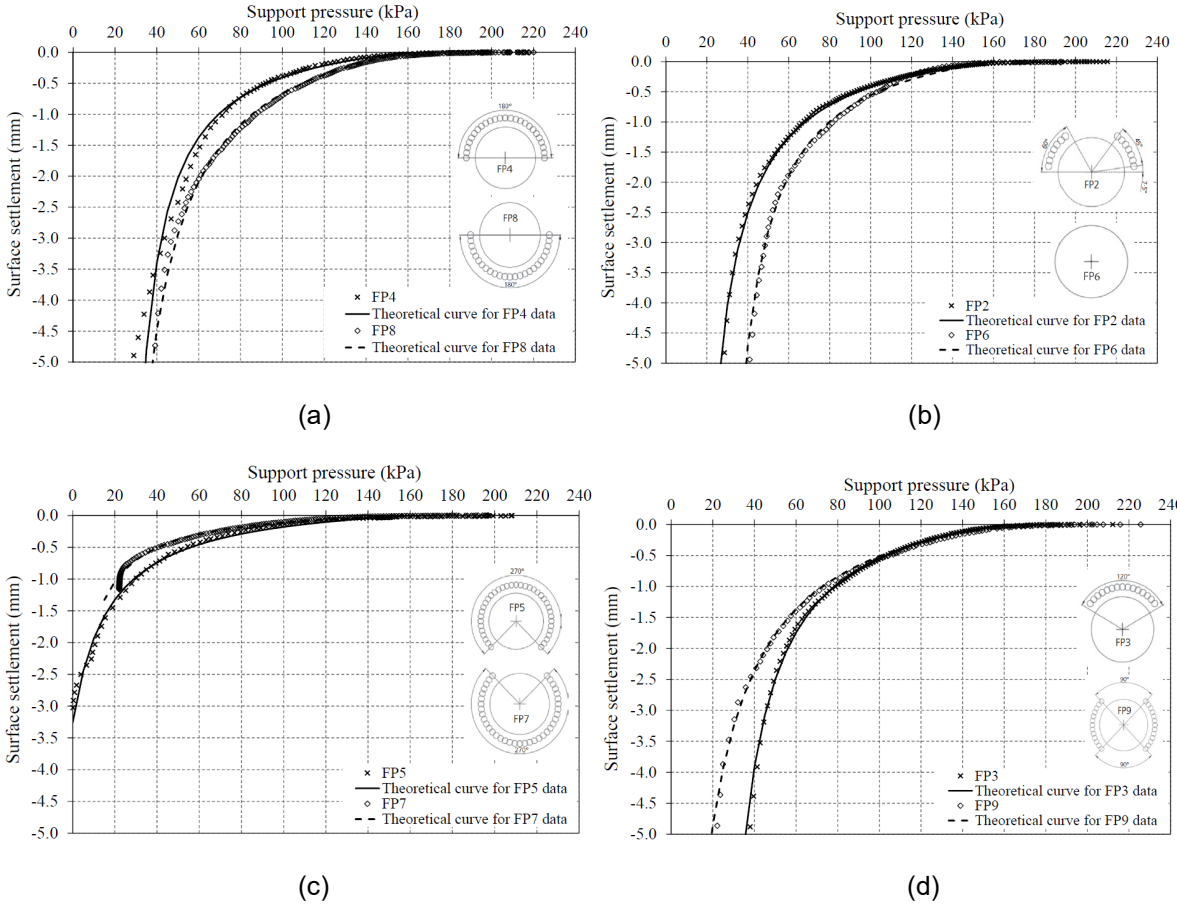

Figure 8. Metro stations layout of Line 5.

Figure 9. Tunnel model geometry (modified from Franco et al., 2019).

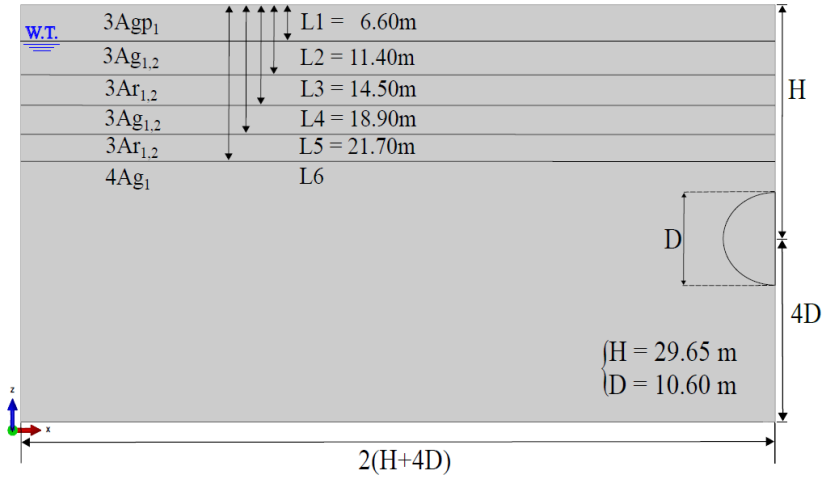

652 Figure 10. Upper and lower bounds of S_{max} between stations HSP and SCR.

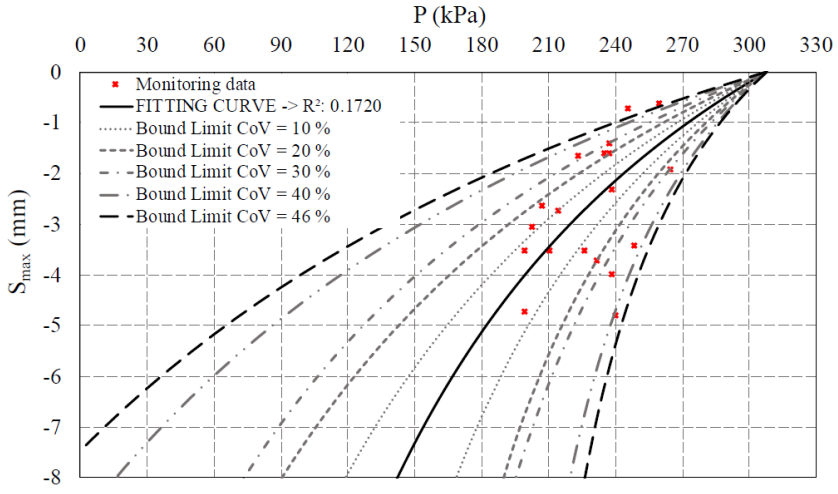

653
654